Int J Thermophys (2008) 29:1408–1421
DOI 10.1007/s10765-008-0489-7

Transport Properties of Undercooled Liquid Copper: A Molecular Dynamics Study

X. J. Han · M. Chen · Y. J. Lü

Received: 11 November 2007 / Accepted: 29 June 2008 / Published online: 6 August 2008

Abstract By using the embedded-atom method (EAM), a series of molecular dynamics (MD) simulations are carried out to calculate the viscosity and self-diffusion coefficient of liquid copper from the normal to the undercooled states. The simulated results are in reasonable agreement with the experimental values available above the melting temperature that is also predicted from a solid–liquid–solid sandwich structure. The relationship between the viscosity and the self-diffusion coefficient is evaluated. It is found that the Stokes–Einstein and Sutherland–Einstein relations qualitatively describe this relationship within the simulation temperature range. However, the predicted constant from MD simulation is close to $1/(3\pi)$, which is larger than the constants of the Stokes–Einstein and Sutherland–Einstein relations.

Keywords Copper · Molecular simulation · Self-diffusion coefficient · Viscosity · Undercooled

1 Introduction

As an example of a metastable state, the undercooled liquid is far from thermodynamic equilibrium. Transport properties, such as the viscosity and the diffusion coefficient, of undercooled liquid metals are significant in the quantitative description of crystal nucleation and growth in metallic melts. They also play an important role in studying the glass transition. Therefore, transport properties of undercooled liquid metals have been receiving extensive research interest. However, despite the considerable experimental and theoretical efforts devoted to these two properties during the last several

X. J. Han · M. Chen (✉) · Y. J. Lü
Department of Engineering Mechanics, Tsinghua University,
Beijing 100084, P.R. China
e-mail: mchen@tsinghua.edu.cn

decades [1,2], there is very limited work in the undercooled liquid regime. The difficulty of experimental efforts lies mainly in two aspects. First, the undercooled state is hard to maintain, because the contact between the metallic melt and the container wall will introduce heterogeneities and thus will induce immediate nucleation of liquid metals [3]. This problem is solved to a certain extent by the development of containerless processing techniques, for example, the electromagnetic levitation (EML) method. Second, the terrestrial determination of transport properties via the EML method experiences large uncertainty. The turbulence inside the droplet under $1g$ conditions affects the measurement of the viscosity and the diffusion coefficient greatly [4]. Accurate measurement of transport properties of undercooled liquid metals may resort to microgravity conditions [5–8]. However, space experiments are often limited due to the cost. It is necessary to develop some predictive method which can give reliable data for liquid metals within the undercooled regime.

Computer simulation with the molecular dynamics method is considered to be one of the most promising methods in this aspect, since it can give information on properties that would be very difficult or even impossible to be obtained by experiments. The embedded-atom model (EAM), originally developed by Daw and Baskes [9,10] on the basis of Stott and Zaremba's earlier quasi-atom concept [11] and Norskov's effective-medium approach [12], has been successfully applied to simulate the structure, thermophysical properties, surface, and phase transformation of solid or liquid metals [13–15]. It has also been applied to predict transport properties of liquid metals [16–20].

In this work, we carried out a thorough EAM-based simulation of a liquid transition metal. Besides the viscosity and the self-diffusion coefficient, some other related properties including the density, the melting point, and the radial distribution function were calculated. The metal we considered is liquid copper. Copper is a simple and model pure metal, but experimental data of these two transport properties within the undercooled regime have not yet been obtained. Brooks et al. [5] once measured the viscosity of liquid copper using an oscillating cup viscometer, but the measurement was limited to the normal liquid state. For the self-diffusion coefficient, only two discrete values exist near the melting temperature. As to the computer simulation, the study of the viscosity and the self-diffusion coefficient was mainly focused on several thermodynamic states near the melting temperature, and there is no systematic investigation of the temperature dependences of these two dynamic properties. For example, in the investigations of Alemany et al. [19,20], only the viscosity and self-diffusion coefficient of liquid copper at 1,423 K was studied with the embedded-atom method (EAM) and with the second-moment approximation to the tight-binding method.

The self-diffusion coefficient can be easily computed from the Green-Kubo (GK) or Einstein equations in the framework of equilibrium molecular dynamics (EMD) simulation. For the viscosity, the computation via EMD often introduces large uncertainty since the result is quite sensitive to the selection of the time origin. Nonequilibrium molecular dynamics (NEMD) simulation methods is applied here to verify the result of EMD and evaluate the prediction accuracy. In normal NEMD [21], the equilibrium viscosity is derived from the data at high shear rates. So, another NEMD technique, the reversed non-equilibrium molecular dynamics (RNEMD) method, was proposed by Müller-Plathe [22–24]. In normal NEMD, the cause is a velocity gradient and the

result is the momentum flux, whereas in the RNEMD technique the momentum flux is given and the velocity gradient is calculated. The advantage of RNEMD is that the momentum and the energy are both conservative, the viscosity is directly computed, and the derivation process from high shear rate as in NEMD is not required. In the present work, the viscosity of undercooled liquid copper will be predicted from these three molecular dynamics simulation methods.

The organization of the rest of the paper is as follows. In the next section, we describe in detail the system studied and the details of the simulations. The simulation results are analyzed and discussed in Sect. 3, and we end with some concluding remarks in Sect. 4

2 Simulation Details

Molecular dynamics simulations are performed with a monatomic system containing 2,048–10,976 atoms under periodic boundary conditions in three coordinate directions. The interactions among all atoms are calculated using the embedded atom method (EAM). According to the EAM potential model, the energy of an atomic system can be written as

$$E_{\text{tot}} = \sum_i F_i\left(\rho_i\right) + \frac{1}{2}\sum_{i\neq j}\phi_{i,j}\left(r_{i,j}\right) \tag{1}$$

$$\rho_i = \sum_{i\neq j} f_j\left(r_{i,j}\right) \tag{2}$$

where F_i is the energy for embedding atom i in an electron density ρ_i, $\phi_{i,j}$ is a two-body central potential between atoms i and j, and $f_j(r_{i,j})$ is the contribution of atom j to the electron density at atom i located at a distance $r_{i,j}$ from atom j.

We employ the model proposed by Mishin et al. [25] in our calculations. The EAM potential of Mishin et al. uses more fitting parameters during construction and includes ab initio energies in the fitting database. So, it is expected to be more suitable to describe the atomic interaction of copper.

The system is first equilibrated at 1,700 K under a constant temperature and constant pressure condition (NPT ensemble). During simulations, the extended system method proposed by Andersen is applied [26]. The equations of particle motion are integrated with the velocity Verlet algorithm at a time step of 1×10^{-15} s. The system is then cooled to the desired temperature with a cooling rate of $2 \times 10^{12}\ \text{K}\cdot\text{s}^{-1}$, during which the pressure is fixed to be zero. At selected temperatures, the dynamic properties are studied in a constant temperature and constant volume condition (NVT ensemble) or a constant volume and constant energy condition (NVE ensemble).

The self-diffusion coefficient D is calculated from the mean-square displacement (MSD) [27], which is given by

$$\left\langle r^2(t)\right\rangle = \frac{1}{N}\sum_{i=1}^{N}\left(|r_i(t) - r_i(0)|^2\right) \tag{3}$$

and

$$D = \lim_{t\to\infty} \frac{1}{6t} \left\langle r^2(t) \right\rangle \tag{4}$$

In order to evaluate the accuracy of the prediction, we utilize three different techniques to calculate the viscosity. One method is to calculate the viscosity from the autocorrelation function of the pressure tensor within the framework of equilibrium MD (EMD). From the linear response theory of Kubo [27], the viscosity is given by

$$\eta = \frac{1}{Vk_bT} \int_0^\infty \left\langle P_{\alpha\beta}(0) P_{\alpha\beta}(\tau) \right\rangle \mathrm{d}\tau \tag{5}$$

where V is the volume, k_b is Boltzmann's constant, T is the absolute temperature, and $P_{\alpha\beta}$ is defined by

$$P_{\alpha\beta} = \sum_{j=1}^{N} \left(\frac{p_{\alpha j} p_{\beta j}}{m_j} + \beta_j F_{j\alpha} \right) \tag{6}$$

and is related to one component of the off-diagonal term of the stress tensor, $\sigma_{\alpha\beta}$, where $\alpha\beta$ equals xz, xy, yz, zx, or zy. $p_{\alpha j}$ and $p_{\beta j}$ are the momenta of particle j in the α and β directions, respectively, β_j is the β component of the jth particle position vector, and $F_{j\alpha}$ is the α component of the force on particle j.

In order to obtain reliable average values for Eq. 3, we utilize a method of overlapping-time-interval correlation averages proposed by Rapaport [28]. The simulations are run using a microcanonical ensemble (constant N, V, and E). Each simulation contains 2,048 atoms. The results for the shear viscosity are calculated using an average of 1,000 individual correlation functions spaced by 0.1 ps. The total time for the correlation function calculation is 4 ps. For each autocorrelation function calculated, the simulations last approximately 100 ps. A total of three to four autocorrelation functions are subsequently averaged to obtain the presented values. The estimated uncertainties in the shear viscosity data are less than 12 %.

The second method is to calculate the viscosity from the direct response to external driving in nonequilibrium MD (NEMD) [21]. The simulated system contains 4,000 atoms. The periodic boundary conditions are applied to the x-y plane. To produce a constant Couette flow in the z direction, the upper cell bordering the fundamental cell being considered moves with a relative velocity of V_x, and the lower cell moves with a relative velocity of V_x in the opposite direction. The shear rate $\gamma = \mathrm{d}V_x/\mathrm{d}z$ has a constant value. The shear viscosity η is given by the relation of the stress tensor P_{xz} and the shear rate γ as follows:

$$\eta = -P_{xz}/\gamma \tag{7}$$

During the simulations, large shear rates ranging from 0.3 to 1.0 in reduced units are used, and the Newtonian shear viscosity is recovered by extrapolating the calculated shear rate of the non-Newtonian viscosity to zero. Since the applied shear rate injects

energy into the system, an additional thermostat is used to conserve the total energy as well as the total linear momentum. Details on this thermostat, the NEMD method, and algorithm used in this paper can be found in Ref. [28].

The third method is the so-called reversed nonequilibrium MD (RNEMD) approach proposed by Müller and Plathe [22–24]. During simulations of an $8 \times 8 \times 16$ (4,096 atoms) system, periodic boundary conditions are applied in the three coordinate directions. The box is subdivided into 20 slabs, the index of which increases from $z = -L_z/2$ to $z = L_z/2$ with L_z the box length in the z direction. In slab 1, the atom has the largest momentum component in the $-x$ direction. Likewise, in slab 11, the atom with the largest momentum component in the $+x$ direction is found. Then the momenta of these two atoms are exchanged. After checking that the system is in the linear response regime, we exchange the momentum every 15 time steps. After a periodic momentum swap of about 3×10^5 time steps at desired temperatures, the system converges toward a steady state. The velocity gradient in the $x$direction is calculated from the average x-velocity in each slab. In the analysis of the velocity profile, we disregard the two slabs in which the momentum exchange takes place. The momentum flux $j_z(p_x)$ is precisely given as

$$j_z(p_x) = \frac{\sum_{\text{exch}} (p_{x,11} - p_{x,1})}{2t L_x L_y}, \tag{8}$$

where t is the simulation time, $p_{x,1}$ and $p_{x,11}$ are the two x components of the exchanged momenta in the slabs 1 and 11, respectively, and L_x and L_y are the lengths of the simulation box in the x and y directions. From the momentum flux and the measured velocity gradient, the shear viscosity can be obtained as

$$\eta = -\frac{j_z(p_x)}{\partial v_x / \partial z} \tag{9}$$

During simulations, for maintaining a constant temperature, the system is coupled weakly to a temperature bath at a frequency of once per 0.1 ps.

The error bar of the predicted shear viscosity in the RNEMD simulation can be given by [24]

$$\frac{\Delta\eta}{\eta} \leq \frac{\Delta J}{J} + \frac{\Delta G}{G} \tag{10}$$

where G is the slope of the linear velocity profile determined with a least-squares fit, and ΔG is the error bar from this fit. According to Eq. 8, flux J is proportional to the exchanged momentum. Once the system is in the steady state, the cumulative exchanged momentum varies linearly with the simulation time. We determine the slope and its error bar by a least-squares fit. The error bar permits us to estimate ΔJ. In the present work, the uncertainty of the shear viscosity is estimated to be about 2.0 %.

Besides the transport properties, we calculate some other related properties such as the melting temperature and the density. The former is indispensable to judge whether the liquid is in the normal regime or in the undercooled regime.

The density can be easily calculated from the mass and the box lengths of the system in a constant temperature and constant pressure (NPT) simulation. The equilibrium melting temperature, T_m, is estimated by a MD simulation of a metastable crystal–liquid sandwich structure and by studying the growth direction of the layers as a function of temperature [29–32]. During the simulations, a $6 \times 6 \times 18$ (2,592 atoms) crystal–liquid–crystal sandwich structure is used and the system along the z axis is divided into 12 layers. The first and the last three layers hold 1,296 solid atoms at 300 K. The intermediate six layers hold the 1,296 liquid atoms at 2,000 K. Then the whole system is allowed to develop at a desired temperature. T_m is evaluated from the change of the growth direction of the computer modeled metastable structure. Above T_m, the system will ultimately turn into a homogeneous liquid, whereas below T_m, the whole system will become a solid phase.

3 Results and Discussions

3.1 Melting Temperature and Density

Figure 1 presents the simulated internal energy E in the homogeneous state when starting at a metastable computer modeled crystal–liquid–crystal sandwich structure. There exists a discontinuity in the E–T curve at $T = (1,322 \pm 1)$K, which corresponds to the melting temperature, T_m. The simulated melting temperature agrees well with the experimental value of 1,356 K [33], with a deviation of $-2.4\,\%$. According to the melting temperature, the simulated undercooling is up to 422 K. The maximum superheating is 378 K.

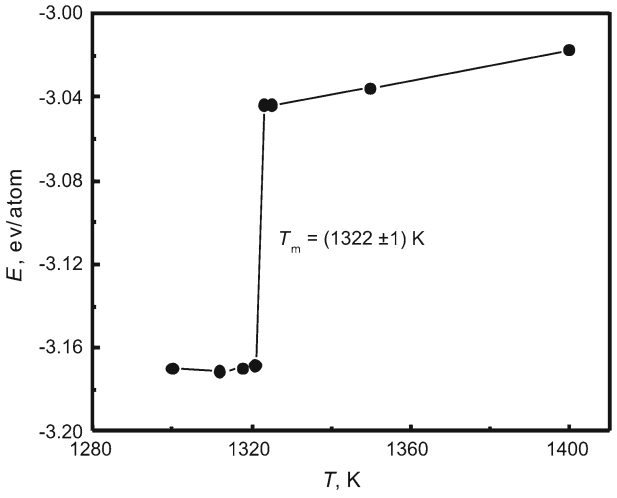

Fig. 1 Calculated sandwich structure internal energy of copper at the end state versus temperature

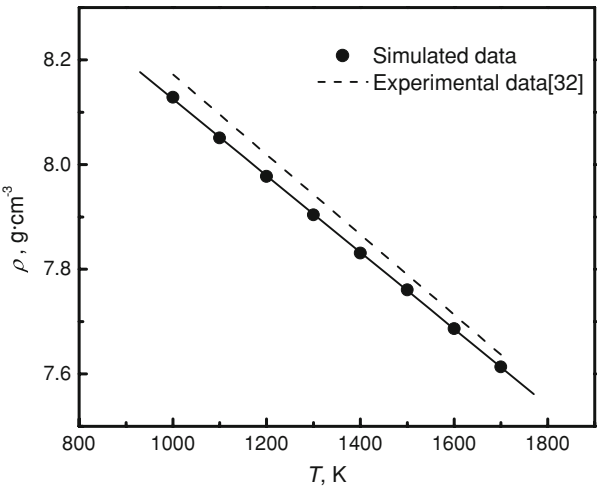

Fig. 2 Density of liquid copper versus temperature. Solid line is the linear fit to the simulated results as Eq. 11, and dash line gives the experimental results as Eq. 12

The simulated density as a function of temperature is illustrated in Fig. 2. A linear regression is given as

$$\rho = 7.89 - 7.32 \times 10^{-4}(T - T_{\mathrm{m,Simu}}) \quad \mathrm{g \cdot cm^{-3}} \tag{11}$$

where $T_{\mathrm{m,Simu}}$ is the simulated melting point and T is the absolute temperature. This is in good agreement with the experimental results given by Brillo and Egry [34], which are denoted by a dashed line in Fig. 2 and represented by

$$\rho = 7.90 - 7.65 \times 10^{-4}(T - T_{\mathrm{m,Exp}}) \quad \mathrm{g \cdot cm^{-3}} \tag{12}$$

where $T_{\mathrm{m,Exp}}$ is the melting point in experiments. The difference between the simulated and experimental values of density is less than 0.56 %.

3.2 Viscosity

During the NEMD calculations, the accuracy of the predicted viscosity depends to a great extent on the function used for extrapolating the shear viscosity to zero shear rate. In this work, we find that the viscosity shear-rate dependence of liquid copper can be well represented by a power function in the entire simulation temperature range:

$$\eta = \eta_0 + A_1 \gamma^{\frac{1}{2}} \tag{13}$$

where η is the shear viscosity, γ is the shear rate, and A_1, and η_0 are the two fitting parameters.

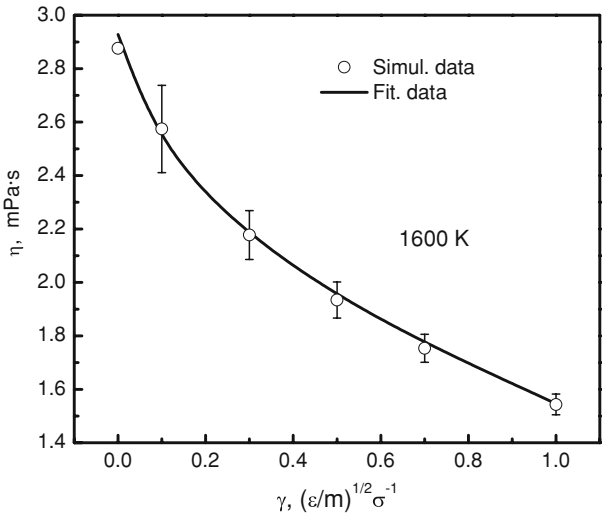

Fig. 3 Viscosity of liquid copper versus the shear rate (reduced units are used, $\sigma = 2.556$ Å, $\varepsilon = 1.602 \times 10^{-19}$ J, and $m = 1.055 \times 10^{-25}$ kg)

As an example, the relationship between the shear viscosity of liquid copper and the shear rate at 1,600 K is presented in Fig. 3. The fitting result of the shear viscosity at 1,600 K is given by

$$\eta = 2.92789 - 1.38156\gamma^{\frac{1}{2}} \quad \text{mPa} \cdot \text{s} \tag{14}$$

with $\gamma = 0$, the equilibrium shear viscosity of liquid copper at 1,600 K is extrapolated as 2.92789 mPa · s. Similarly, the equilibrium shear viscosities at different temperatures can be obtained.

Figure 4 illustrates the x-component velocity profiles in the RNEMD simulations. For clarity, only velocity profiles of five temperatures are presented in this figure. Due to the periodic boundary condition, the velocity profile is antisymmetric as to slab 11, which corresponds to the minimum of the velocity profile at a given temperature. Obviously, the velocity profile from slab 2 to slab 10 is approximately linear, and a linear regression only brings about an uncertainty less than 0.9 %. Based on the measured velocity gradient and the imposed momentum flux, the shear viscosity of liquid copper at a desired temperature can be obtained according to Eq. 9.

In Fig. 5, we report our results as well as the experimental values determined by Egry et al. above the melting temperature [5]. The viscosities calculated from NEMD, RNEMD, and EMD simulations are plotted as open squares, solid circles, and open circles, respectively. The solid triangles denote the experimental viscosity of Egry et al. Noteworthily, the results of EMD, NEMD, and RNEMD methods are mutually consistent. Moreover, the predicted shear viscosities from these three techniques are in reasonable agreements with experimental data above the melting point, and the differences are about 11 %, 14 %, and 15 %, respectively, for NEMD, RNEMD, and EMD methods at 1,400 K. The viscosity of liquid copper seems to follow the Arrhenius

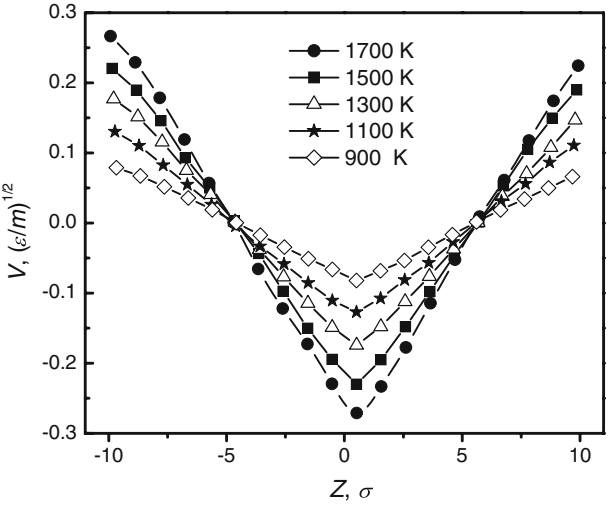

Fig. 4 Velocity profiles in the simulation cell (reduced units are used)

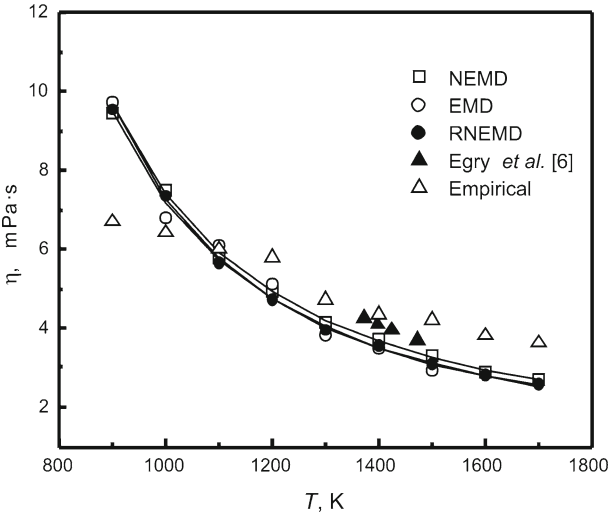

Fig. 5 Viscosity of liquid copper at different temperatures

relationship in the simulation temperature range:

$$\eta = \eta_0 \exp\left(\frac{E_a}{k_b T}\right) \tag{15}$$

where η_0 is the prefactor, k_b is Boltzmann's constant, and E_a is the activation energy. In Table 1, we present the values for the activation energy as well as the prefactors for each method.

Table 1 Viscosity parameters assuming Arrhenius behavior for each method

Methods	η_0(mPa · s)	E_a/k_b(K)
NEMD	0.5765	2, 591.23
RNEMD	0.5416	2, 624.62
EMD	0.5566	2, 570.48
Experimental	0.5259	2, 867.87

It is interesting to evaluate a frequently used empirical expression, which estimates the viscosity from the radial distribution function, $g(r)$ [35]:

$$\eta \approx 4.5 v_0 P(T) m n_0^2 g(r_m) r_m^5 \left(1 - r_0/r_m\right) \tag{16}$$

where m is the atomic mass, n_0 is the atomic density, v_0 is a characteristic constant, r_m and r_0 are the positions of the first peak and its left-hand edge in the $g(r)$ curve, respectively, and $P(T)$ is given by

$$P(T) = 1 - \int_{\varphi}^{\infty} (2\pi)^{-1/2} \exp\left(-\frac{\varphi^2}{2}\right) \mathrm{d}\varphi \tag{17}$$

with

$$\phi = \frac{\sqrt{3}}{2}\left(\frac{T_b - T}{T}\right) \tag{18}$$

For copper, v_0 and T_b are $3.54 \times 10^{12} s^{-1}$ and 2,903 K [35], respectively.

The simulated RDFs at different temperatures are shown in Fig. 6. The reasonability of simulated results can be illustrated from the good agreement with the experimental RDF at 1,783 K [36], which is denoted by open circles. The RDFs presented here are calculated for 2,000 different configurations of 4,096 atoms.

The calculated viscosity from Eq. 16 is represented by open triangles in Fig. 5. Generally speaking, the empirical expression predicts similar temperature dependence and comparable values of viscosity with the MD simulations. However, it should be noted that at temperatures below 1,200 K the temperature dependence of viscosity empirically estimated deviates from the simulated one. This deviation may be ascribed to the short cutoff distance in the EAM model. From the simulated RDFs at different temperatures, we can see that the lower the temperature, the more intense is the correlation of atoms at longer distances. Therefore, the approximation can be improved if a larger cutoff distance is considered.

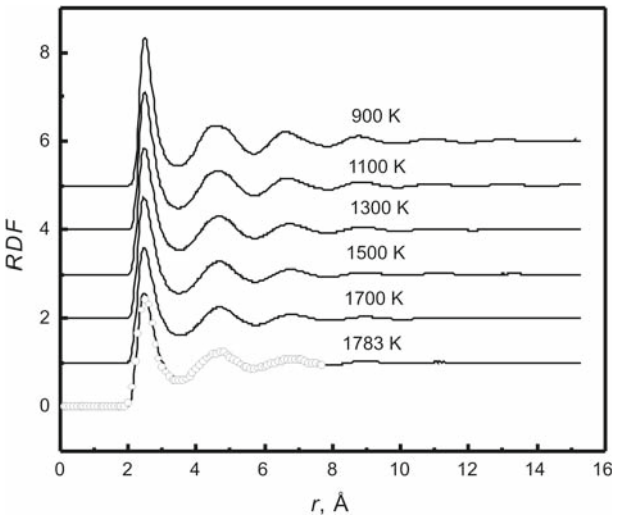

Fig. 6 Radial distribution functions of liquid copper at different temperatures. Open circles denote the experimental results at 1,783 K

3.3 Self-Diffusion Coefficient

The mean square displacements (MSDs) of liquid copper at different temperatures are shown in Fig. 7. In these curves, two time regimes can be distinguished. For short times, the motion of the particle is ballistic, and the MSD is proportional to t^2. For long times, the motion is diffusive and the MSD is proportional to t. From the first derivative of the MSD in the diffusive regime, the self-diffusion coefficient is obtained according

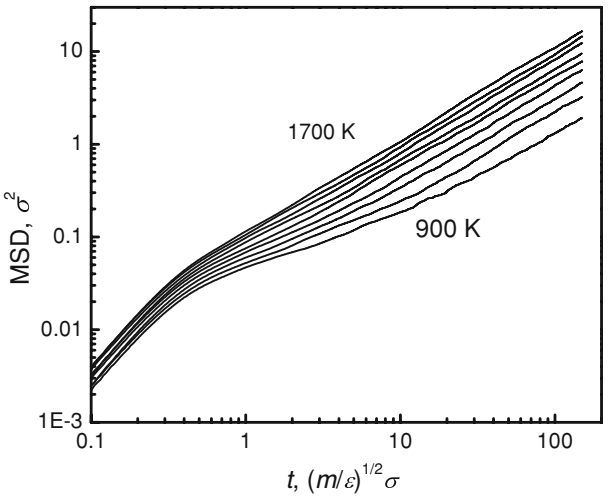

Fig. 7 MSDs of liquid copper at different temperatures (reduced units are used)

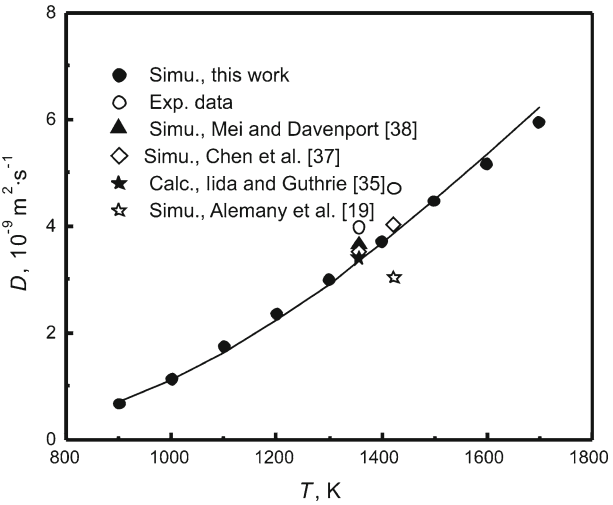

Fig. 8 Self-diffusion coefficient of liquid copper versus temperature. Solid line describes the Arrhenius fit to the simulated results

to Eq. 4. The simulated self-diffusion coefficients in this work and those from other studies are presented in Fig. 8. The solid circles denote the simulated results in the present work, and the open ones are the experimentally determined values. The open squares and the solid triangle represent the simulated values from the EAM potentials by Chen et al. [37] and from Mei and Davenport [38], respectively. The solid star is the predicted self-diffusion coefficient of Iida from an empirical expression [35], and the open star denotes the simulated result for liquid copper by Alemany et al. [19] at 1,423 K. Comparisons show that at 1,357 K the simulated data in the present work are very close to the predicted values from the EAM models by Chen and Mei, the difference being −1.2 % and −4.9 %, respectively. The results in this work agree also well with the predicted values of Iida with a deviation of about 2 %. Meanwhile, our computation results are in reasonable agreement with the experimental data, and the deviation is about −12 %. An Arrhenius best fit shows that the self-diffusion coefficient is related to the temperature by

$$D = 7.3828 \times 10^{-8} \cdot \exp\left(-\frac{4,200.51}{T}\right) \quad \mathrm{m}^2 \cdot \mathrm{s}^{-1}, \tag{19}$$

and the result is plotted as the solid line in Fig. 8.

On the basis of the simulated viscosity and the self-diffusion coefficient, we investigate the relationship between the two transport properties. The value of $DR\eta/(k_\mathrm{b}T)$ is evaluated, where the atomic radius R is calculated from the predicted atomic density. As shown in Fig. 9, $DR\eta/(k_\mathrm{b}T)$ of liquid copper changes little with the variation of temperature, which is in the range of 0.092–0.099. This value is very close to $1/(3\pi)$, and is remarkably larger than the predicted constant $1/(6\pi)$ of the Stokes–Einstein expression [39] and $1/(4\pi)$ of the Sutherland–Einstein expression [40].

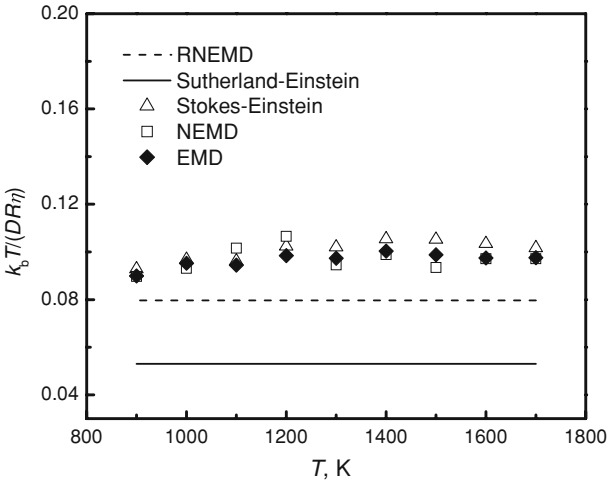

Fig. 9 Calculated $DR\eta/(k_bT)$ for liquid copper at different temperatures

4 Conclusions

With molecular dynamics simulation and the EAM potential model, the transport properties of liquid copper are calculated. The melting temperature of copper is evaluated from a crystal–liquid sandwich structure. The self-diffusion coefficient is predicted from EMD simulations, and the viscosity is computed from three different simulation techniques, namely, EMD, NEMD, and RNEMD simulations. The results from the three simulation methods are mutually consistent. In the simulation, the temperature dependences of both the viscosity and the self-diffusion coefficient can be well represented by the Arrhenius relation. The simulated transport properties are in good agreement with the available experimental data. The Stokes–Einstein or Sutherland–Einstein relation could be applied to describe the relationship between the viscosity and the self-diffusion coefficient. However, the constant is recommended to be $1/(3\pi)$ instead of $1/(6\pi)$ or $1/(4\pi)$ for liquid copper.

Acknowledgments This work was financially supported by China Postdoctoral Science Foundation and the National Natural Science Foundation of China under grant Nos. of 50395101 and 50371043. The computations are carried out at the Tsinghua National Laboratory for Information Science and Technology, China. The authors are grateful to Mr. D. Q. Yu for valuable discussions.

References

1. L. Battezzati, G. S. Greer, Acta Metall. **37**, 1791 (1989)
2. M. Shimoji, T. Itami, in *Diffusion and Defect Data*, ed. by F.H. Wohlbier (Trans Tech, Aedermannsdorf, Switzerland, 1986)
3. X.J. Han, B. Wei, Philos. Mag. **83**, 1511 (2003)
4. D.M. Herlach, R.F. Cochrane, I. Egry, H.J. Fecht, A.L. Greer, Int. Mater. Rev. **38**, 273 (1993)
5. R.F. Brooks, I. Egry, S. Seetharaman, D. Grant, High Temp.-High Press. **33**, 631 (2001)
6. I. Egry, G. Lohofer, I. Seyhan, S. Schneider, B. Feuerbacher, Appl. Phys. Lett. **73**, 462 (1998)

7. I. Egry, J. Non-Cryst. Solids **250**, 63 (1999)
8. B.N. Antar, E.C. Ethridge, D. Maxwell, Microgravity Sci. Technol. **14**, 9 (2003)
9. M.S. Daw, M.I. Basker, Phys. Rev. Lett. **50**, 1285 (1983)
10. M.S. Daw, M.I. Baskes, Phys. Rev. B **29**, 6443 (1984)
11. M.J. Stott, E. Zaremba, Phys. Rev. B **22**, 1564 (1980)
12. J.K. Norskov, Phys. Rev. B **26**, 2875 (1982)
13. U.K. Röβler, H. Teichler, Phys. Rev. E **61**, 394 (2000)
14. H. Teichler, Phys. Rev. E **53**, 4287 (1996)
15. L. Wang, X.F. Bian, J.X. Zhang, J. Phys. B At. Mol. Opt. **35**, 3575 (2002)
16. F.J. Cherne, M.I. Baskes, Phys. Rev. B **65**, 024209 (2001)
17. M.M.G. Alemany, C. Rey, L.J. Gallego, J. Chem. Phys. **109**, 3568 (1998)
18. M.M.G. Alemany, C. Rey, L.J. Gallego, Phys. Rev. B **58**, 685 (1998)
19. M.M.G. Alemany, C. Rey, L.J. Gallego, J. Chem. Phys. **109**, 5175 (1998)
20. M.M.G. Alemany, O. Diéguez, C. Rey, L.J. Gallego, Phys. Rev. B **60**, 9208 (1999)
21. D.J. Evans, G.P. Morriss, *Statistical Mechanics of Non-equilibrium Liquids* (Academic, London, 1990)
22. F.Müller-Plathe, J. Chem. Phys. **106**, 6082 (1997)
23. F.Müller-Plathe, Phys. Rev. E **59**, 4894 (1999)
24. P. Bordat, F.Müller-Plathe, J. Chem. Phys. **116**, 3362 (2002)
25. Y.Mishin, M.J. Mehl, D.A. Papaconstantopoulous, A.F. Voter, J.D. Kress, Phys. Rev. B **63**, 224106 (2001)
26. H.C. Andersen, J. Chem. Phys. **72,** 2384 (1980)
27. D.A. McQuarrie, *Statistical Mechanics* (Harper and Row, New York, 1976)
28. D.C. Rapaport, *The Art of Molecular Dynamics Simulation* (Cambridge University Press, Cambridge, 1995)
29. S. Toxvaerd, E. Praestgaard, J. Chem. Phys. **67**, 5291 (1977)
30. Y. Hiwatari, E. Stoll, T. Schneider, J. Chem. Phys. **68**, 3401 (1978)
31. H. Teichler, Phys. Rev. B **549**, 8473(1999)
32. X.J. Han, M. Chen, Z.Y. Guo, J. Phys.: Condens. Matter **16,** 705 (2004)
33. C.J. Smithell, *Smithells Metals Reference Book*, ed. by E.A. Brandes (Butterworths, London, 1983), p. 14-6
34. J.Brillo, I. Egry, Z. Metallkd, **95**, 691 (2004)
35. T. Iida, R.I.L.Guthrie, *The Physical Properties of Liquid Metals* (Claredon, Oxford, 1993)
36. Y. Waseda, *The Structure of Non-crystalline Materials: Liquids and Amorphous Solids* (McGraw-Hill, New York,1980)
37. F.F. Chen, H.F. Zhang, F.X. Qin, Z.Q. Hu, J. Chem. Phys. **120**, 1826 (2004)
38. J. Mei, J.W. Davenport, Phys. Rev. B **42**, 9682 (1990)
39. A. Einstein, *Investigations on the Theory of Brownian Movement* (Dover, New York, 1956)
40. W. Sutherland, Philos. Mag. **9**, 781 (1905)